The NASA Turbulent Heat Flux Experiments: Summary and Lessons Learned

Nicholas J. Georgiadis,[1] Mark P. Wernet,[2] and Michael R. Borghi[3]
NASA Glenn Research Center, Cleveland, OH 44135

Chad M. Winkler[4]
The Boeing Company, St. Louis, MO 63042

Michael A. Emory[5]
Luminary Cloud, San Mateo, CA 94401

Randy J. Locke[6]
HX5 LLC, Cleveland, OH, 44135

This extended abstract is for a paper proposed for the AIAA 2026 Aviation Conference that will provide an overview of the NASA Turbulent Heat Flux (THX) experiments. The THX experimental work was conducted at NASA Glenn Research Center (GRC) in order to collect measurements of velocities and temperatures for computational fluid dynamics (CFD) validation of heated flows, with a focus on propulsion system components. The experiments spanned 5 phases; four of which were conducted in the GRC Aeroacoustic Propulsion Laboratory (AAPL) using the Small Hot Jet Flow Rig (SHJAR). In addition, computational studies were also conducted for each of the experimental configurations, in order to provide a baseline of expected CFD results and to make an assessment of the capability of various CFD approaches for calculating flows where the turbulent transport of heat was important. Two of the collected sets of data were used for American Institute of Aeronautics and Astronautics (AIAA) Propulsion Aerodynamic Workshops (PAWs). The data set from the 5th phase, collected for heated supersonic jets, was also used to construct new validation cases for the NASA Turbulence Model Resource (TMR). The final paper will provide more details than those outlined here, overall lessons learned, and recommendations for future experimental and computational efforts to advance capabilities for predicting turbulent flows where thermal transport is important.

Introduction

Flow turbulence has been recognized by the aerospace research and development (R & D) community as one of the most important factors affecting aerospace system performance and one of the most difficult physical phenomena to understand and predict. Computational fluid dynamics (CFD) technologies have become widely used in the R & D community, and while there have been continual advances in computing capability, the ability to simulate complex aerospace flows is limited by the ability to replicate the effects of turbulence. A primary shortcoming has been the lack of validation data with sufficient details needed to understand the effects of turbulence and identify trends that can result in improved computational models for turbulence. These details include measurements of important mean flow quantities and turbulent statistics with sufficient spatial resolution, but also enough geometry and flow condition information (i.e. boundary conditions) to adequately model the flow problems of interest. In the study of Slotnick et al.[1], it was concluded that improving techniques for computing turbulent flows remains of paramount importance, and that there is a need for experimental testing programs that are planned with computational turbulence modeling development and validation activities in mind.

[1] Aerospace Engineer, Inlets and Nozzles Branch, Georgiadis@nasa.gov, AIAA Associate Fellow
[2] Senior Research Engineer, Optics and Photonics Branch, Mark.P.Wernet@nasa.gov, AIAA Associate Fellow
[3] Aerospace Engineer, Turbomachinery and Turbolelectric Systems Branch, Michael.R.Borghi@nasa.gov, AIAA Member
[4] Boeing Technical Fellow, Chad.M.Winkler@boeing.com, AIAA Associate Fellow
[5] Product Manager, memory@luminarycloud.com, AIAA member.
[6] Research Engineer, retired, rjlocke66@gmail.com.

In recent years, research into improving turbulence modeling has been sponsored by NASA's Transformational Tools and Technologies (TTT) project of NASA's Transformative Aeronautics Concepts Program (TACP). This research has consisted not only of advanced computational method development and validation, but also fundamental experiments with detailed measurements needed to make computational modeling assessments. Historically, work into turbulence modeling for problems where turbulent heat flux is important has been rather limited. Turbulent temperature variations and heat flux are prevalent in high Mach number applications, propulsion systems, and systems that require active cooling, just to name a few. There had been a lack of experimental data to improve and validate such models, which is primarily due to the difficulty of obtaining detailed time-resolved measurements of temperature where there is turbulent transport of heat. As discussed in Refs. [2-4], standard Reynolds-averaged Navier-Stokes (RANS) based techniques perform poorly when considering prediction of turbulent heat flux and temperatures in propulsion flows involving turbulent shear layers. Scale-resolving simulation (SRS) methods, utilizing large-eddy simulation (LES) for all or a portion of the flow, have begun to be used for more complex problems, but are still limited by the computational resources required for such calculations. The standard practice for computational analysis of heated propulsion flow components had been to use two-equation RANS models for the in-flow aerodynamics and thermodynamics, including constant turbulent Prandtl number modeling for the turbulent heat flux and then employ relatively simple boundary conditions for wall surface temperatures or heat flux.

To address the shortfall of experimental data available to improve and validate turbulence modeling for flows where turbulent thermal transport is important, the TTT project sponsored a series of test campaigns referred to as the Turbulent Heat Flux (THX) experiments. In this proposed paper for the AIAA Aviation 2026 Conference, the authors will summarize the entire THX experimental effort, which consisted of five separate phases. Two of the phases provided data that were utilized in AIAA Propulsion Aerodynamic Workshops (PAWs). In this extended abstract, we give a very brief overview of each of the phases. The final paper will provide more of the key details, overall lessons learned, and recommended areas of future research in the field of advancing turbulence modeling for high-energy, thermally-dominated flows.

THX Experimental Phases

1. Low-speed and low-temperature film cooling

The first phase of the THX experiments were low-speed / low-temperature cooling hole investigations in the NASA Glenn Research Center (GRC) Fundamental Film Cooling and Heat Transfer Facility (SW6). Figure 1 shows a schematic of the facility with the primary air inflow and configuration with three injector flows. For convenience in these fundamental flow measurements, the injected flow is actually heated in the SW6 configuration, and the primary air is at room temperature, which is in contrast to a typical film-cooling arrangement where the injected flow is at lower temperature and designed to provide a layer of air colder than the primary stream to cover and protect the surface, whether it be a turbine blade, engine combustor, or nozzle afterbody. Hot-wire anemometry and Particle-Image Velocimetry (PIV) were used to make measurements as documented in Refs. 5 and 6. This was the one phase of the THX experiments where the actual heat flux quantity (or u'T') was measured. Borghi et al.[7] performed calculations of the configuration with RANS, hybrid RANS-LES, and LES. An instantaneous snapshot of the flow computed from LES is shown in Fig. 2. A comparison of experimental and computed rms of temperature is provided in Fig. 3. The experimental results showed that periodicity could be assumed with reason and the computations only computed a single cooling hole with periodic boundary conditions in the spanwise direction. The results show close agreement between the measurements and computations.

2. Subsonic convergent nozzles

Phases 2-5 were all conducted in the GRC Aeroacoustic Propulsion Laboratory (AAPL) using the Small Hot Jet Acoustic Rig[8-9] (SHJAR). A photograph of the SHJAR with one of the Phase 5 C-D nozzles (Phase 5) installed in the facility is shown in Fig. 4. For subsonic jets exhausting from round convergent nozzles, a broadly used set of PIV data was collected by Bridges and Wernet[10-11] several years prior to the THX effort. Jet data were collected for operating points at several Mach number and temperature settings. PIV data for three of these operating points had been used to create subsonic jet validation cases for the NASA Turbulence Modeling Resource (TMR).[12] The data sets consisting of mean velocities and turbulent statistics were augmented in the second THX phase with temperature data taken with a new rotationally resolved Raman spectroscopy technique developed by Locke et al.[13] This Raman technique will be described more thoroughly in the final paper. The same nozzle and many of the same operating points from Refs. 10-11 were utilized to obtain measurements of mean and rms temperatures in the jet plumes.

DeBonis[14] obtained LES calculations of select subsonic test points from consensus data and compared computed solutions to the previously collected PIV data and the temperature data collected during the second phase of the THX experiments. An older data set obtained by Mielke et al.[15] using the Rayleigh measurement technique to obtain temperatures but also collected in the GRC SHJAR, was also used in Debonis's comparisons. A comparison of experimental and computed mean temperature and rms of temperature is provided in Fig. 5.

3. Single Cooling Hole Experiments

PIV measurements for velocities and Raman-based temperature measurements were made for the fundamental configuration of a square nozzle producing heated subsonic flow over a plate with a single large injector cooling flow as described in Wernet et al[16]. The experimental configuration is shown in Fig. 6. The convergent nozzle, with a square exit, transitioned from the upstream round pipe that joined the SHJAR supply pipe, via a series of super ellipses. The single cooling hole, with a 12.7 mm diameter, was inclined at 30 degrees to the primary stream direction, and had an L/D of 40 to enable a fully developed pipe flow to exit at the plate surface and hence facilitate computational boundary condition settings for CFD validation efforts using this data. Standard two-component PIV measurements were taken through the center-plane of the nozzle, also passing through the centerline of the injector nozzle. Three-component stereo PIV (SPIV) planar measurements were obtained at several planes downstream of the nozzle exit.

Computational simulations were obtained with both wall-resolved LES (WRLES) and RANS calculations as documented in Refs. 17-20. The two LES approaches used very different algorithms. The FDL3DI solver is based upon a high-order compact scheme designed for structured grids. The Glenn Flux Reconstruction (GFR) code also employs a high-order method, but it is the Flux Reconstruction scheme, designed for unstructured methods. For comparison with the two LES results, a RANS result using a Reynolds-stress model in the FUN3D code was chosen from those studied in Ref. 19, as this RANS approach enabled better prediction of three-dimensional turbulent flow structures than linear one- and two-equation turbulence models.

Figure 7 provides instantaneous axial velocity contours for blowing ratios (BR) of 1 and 2 from WRLES calculations using the FDL3DI code. The BR=1 flow enables more of an attached cooling film while the BR=2 flow results in more of a detached inclined jet-in-crossflow situation. A comparison of temperatures from the experiment with the two LES approaches and the Reynolds-stress model RANS approach is provided in Fig. 8. It may be observed that the two LES approaches agree well with each other and better with experiment than the RANS approach. The RANS computed flow results in a cooling jet that does not mix as quickly as indicated by experiment nor the LES approaches. In the final paper, we will present more findings that show the superiority of LES over RANS for prediction of this canonical film cooling experiment. Very notably, the prediction of the actual turbulent heat flux quantities (u'T' and v'T') in the energy equation was found to be much more directionally dependent in the RANS computations than that directly calculated with LES.

4. Film-Cooling Hole Experiments

The same nozzle from Phase 3 of the THX experiments was used in Phase 4. However, instead of the simple plate with single cooling hole, a dual plenum film cooling system was attached to the nozzle in order to provide an arrangement with heated exhaust over a film-cooled plate, as shown in Fig. 9. The plate was cooled with three sections of film-cooling patches each having 45 holes inclined at 30° to the heated primary stream direction. These holes were 1 mm in diameter, much smaller than that of the Phase 3 experiments, and more realistic in terms of what was required to produce a cooling film over the plate. Experimental techniques similar to those of Phase 3 were employed for the Phase 4 experiments, namely PIV measurements for velocities and Raman-based measurements for in-flow temperatures. A background-oriented Schlieren measurement system was used during initial tests to identify the thickness of the cooling film over the plate for various flow conditions, and in turn was used to define and optimize the spatial matrix where the individual point Raman temperature measurements should be made. Surface infrared temperature measurements were also acquired during the Phase 4 tests. The experimental measurements are documented in Refs. 21-22.

Similar to the other phases, computational efforts accompanied the experimental measurements for the THX – Phase 4 configuration. The American Institute of Aeronautics and Astronautics (AIAA) 5th Propulsion Aerodynamic Workshop (PAW5) used this configuration as the nozzle problem. One of the key areas of investigation was determining whether CFD computations with a conjugate heat transfer (CHT) approach were required to obtain accurate calculations of surface temperatures. Figure 10 shows a typical comparison of CFD applied to the configuration with and without CHT and clearly shows that the combined approach is required to provide accurate calculations of film-cooled surface temperatures. Several individual computational investigations from the AIAA PAW5 are presented in Refs. 23-27 and a summary of all the results is presented in Ref. 28. Beyond the surface temperature comparisons, an additional key finding was in the prediction of in-flow temperatures using RANS versus

LES-based techniques. In Fig. 11, a comparison of measured and computed thermal boundary layers is made at 270 mm from the nozzle exit, which is on the overhang of the plate shown in Fig. 9, downstream of the last patch of cooling holes. The RANS solutions as a whole did not replicate the thermal boundary layers nearly as well as the scale-resolving (LES-based) solutions did. In addition to the inferior prediction of the interaction of the cooling flow jets with the heated flow, the Reynolds analogy used in the RANS approach to relate thermal transport to momentum transport, with standard gradient diffusion approximation and a simplistic constant turbulent Prandtl number setting, is not sufficient to yield accurate results.

5. Supersonic Jet Mixing

The same PIV and Raman measurement techniques used in Phases 1-4 were used to obtain detailed aerodynamic and thermodynamic data for turbulent supersonic jets. Operating points from the work of Seiner et al[29] for heated Mach 2 jets were used as a starting point for the matrix of cases examined here using a geometrically similar Mach 2 nozzle. Figure 4 shows the nozzle installed in the GRC SHJAR facility. Two additional nozzles were examined having design Mach numbers of 1.36 and 1.63. For each Mach number, multiple jet temperatures were investigated. Jet measurements were first made with stagnation pressure and temperature probes for comparison to the previous experiments. Experimental results showed that as jet Mach number increases, the overall jet mixing rate decreases, as indicated by the potential core length, downstream mean velocities, and turbulence levels. Similar behavior was observed in the mean temperatures and rms temperatures. The suppression of turbulence as the jet Mach number increases is due to compressibility. For a fixed jet Mach number, increasing the jet temperature resulted in faster mixing by all measures. Peak turbulent stress levels, located along the lipline of the jet, demonstrated trends in individual stress components that differed depending on whether jet Mach number or temperature was varied, but indicated that the turbulence structure parameter (u'v' / k) was very similar when varying either jet temperature or Mach number. The experimental results are presented in detail in Refs. 30-32.

The THX5 supersonic jet data set was used as the nozzle case in the 6th AIAA PAW. Similar to the 5th PAW, a variety of RANS and LES approaches were attempted for the supersonic jet cases. Figure 12 shows a typical result obtained with two-equation RANS for subsonic and supersonic jets. The supersonic jet experimental data was collected in THX5, while the subsonic data was collected prior to the THX experiments, and documented in Refs. 10-11. All of the jet data was collected in the same GRC SHJAR facility with nozzles having the same exit diameter, and using the same measurement techniques. Therefore comparing these subsonic and supersonic jet data sets, albeit collected many years apart, should enable direct comparison concentrating on fluid physics differences. In Fig. 12, examining only the experimental data while first holding the jet exit temperature fixed, suppression of turbulence due to compressibility results in the supersonic jets mixing more slowly than low subsonic jets. When holding jet exit Mach number nearly fixed, it is observed that a heated jet will mix more quickly than an unheated (or more correctly termed temperature matched case for the supersonic jets) jet case. Standard RANS approaches have no capability to capture the effects of compressibility in even simple round jets like these, while at least the trends due to temperature effects are captured to some extent.

In the workshop, some of the participants investigated RANS with compressibility corrections. These corrections have been available for approximately 3 decades, and while in some cases they are able to replicate the trends of reduced mixing rates as jet Mach number increases, they are based on empirical findings and are also used with underlying RANS models that do not replicate key features of an actual jet such as the initial mixing rate and intermittency of turbulence near the end of the potential core. In contrast, highly resolved LES does appear to capture the actual flow physics more accurately, as indicated by the WMLES predictions obtained with the Charles code shown in Figs. 13 and 14. For the jet cases operated on-design and shown in Fig. 13, LES is able to replicate the effects of both jet compressibility and jet heating. Figure 14 shows comparisons for one of the off-design jet cases measured during the THX5 experimental campaign. A summary paper on the PAW6 results appears in Ref. 33, with more comprehensive details of several of the investigations provided in Refs. 34-37.

Three new supersonic jet cases were built for the NASA Turbulence Modeling Resource (TMR) and were taken from the PAW6 nozzle test problem. The three jet cases all used a Mach 1.63 axisymmetric nozzle: a heated jet for each at on-design condition, a temperature-matched on-design condition at Mach 1.63, and an off-design heated condition for the Mach 1.63 nozzle. RANS solutions were obtained using three established Reynolds-averaged Navier-Stokes (RANS) codes: Wind-US, FUN3D, and VULCAN-CFD, all using the Menter Shear Stress Transport k-ω turbulence model with vorticity source term (SST-V). The NASA TMR requires at least two CFD codes yielding essentially identical results to certify that the approaches are verified, meaning that they solve the posed CFD equations as intended. The three codes generally provided very close agreement with each other for jet plume quantities, with the only exception being static temperature. This discrepancy was determined to be the result of whether or not turbulent kinetic energy was considered in the definition of total energy.

The links for all of the cases, with computational grids, experimental data, and sample computational results as documented in a summary report (Ref. 38) of the new TMR cases are as shown below:

AJM163TM: Temperature-Matched Mach 1.63 Axisymmetric Jet:
https://turbmodels.larc.nasa.gov/jet_mach1p63_tmatched_val.html
AJM163H: Heated Mach 1.63 Axisymmetric Jet:
https://turbmodels.larc.nasa.gov/jet_mach1p63_hot_val.html
AJM163OD: Off-Design Mach 1.63 Axisymmetric Jet:
https://turbmodels.larc.nasa.gov/jet_mach1p63_offdesign_val.html

Plans for Final Paper

The final paper will provide more key details of the five THX experimental phases, with emphasis on primary lessons learned from the experimental findings and comparisons to computations. Two of the most significant findings are (1) the inadequacy of RANS to predict details of thermal mixing and thermal boundary layer growth, and (2) the necessity to couple a CFD solver with a CHT solver for conduction heat transfer for calculation of surface temperatures of heated aerospace components, with or without active cooling. Additionally, this paper will serve as an archival source of the entire THX campaign results for those wishing to use the data for thermal modeling.

Acknowledgments

The authors would like to thank participants of the 5th and 6th AIAA PAW for their contribution of solutions that made the comparisons of computational solutions to experimental measurements described in this extended abstract and the final paper possible. The work of the NASA authors was supported by the Transformational Tools and Technologies (TTT) Project of NASA's Transformative Aeronautics Concepts Program (TACP).

References

1. Slotnick, J., Khodadoust, A., Alonso, J., Darmofal, D., Gropp, W., Lurie, E., and Mavriplis, D., "CFD Vision 2030 Study: A Path to Revolutionary Computational Aerosciences," NASA/CR 2014-218178, Mar. 2014.
2. Yoder, D. A., "Comparison of Turbulent Thermal Diffusivity and Scalar Variance Models," AIAA Paper 2016-1561, Jan. 2016, https://doi.org/10.2514/6.2016-1561 .
3. Georgiadis, N. J., Yoder, D. A., Vyas, M. A., and Engblom, W. A., "Status of Turbulence Modeling for Hypersonic Propulsion Flowpaths," *Theoretical and Computational Fluid Dynamics*, Vol. 28, No. 3, 2014, pp. 295–318, https://doi.org/10.1007/s00162-013-0316-z .
4. Yoder, D. A., DeBonis, J. R., and Georgiadis, N. J., "Modeling of Turbulent Free Shear Layer Flows," *Computers & Fluids*, Vol. 117, 2015, pp. 212-232, https://doi.org/10.1016/j.compfluid.2015.05.009.
5. Wernet, M.P., Wroblewski, A.C., and Locke, R.J., "A Dual-Plane PIV Study of Turbulent Heat Transfer Flows," NASA TM-2016-219074, May 2017, https://ntrs.nasa.gov/api/citations/20160003685/downloads/20160003685.pdf.
6. Poinsatte, P., Thurman, D., and Lucci, B., "Detailed Velocity, Temperature, and Heat Flux Measurements on a Large Scale Film Cooling Model,," NASA TM 20220004085, May 2022, https://ntrs.nasa.gov/api/citations/20220004085/downloads/TM-20220004085.pdf.
7. Borghi, M., Thurman, D., Poinsatte, P., and Engblom,W., "Numerical and Experimental Investigation of a Heated Jet in Crossflow," J. Thermophysics and Heat Transfer, Vol.34, No. 2, April 2020, pp. 230-242. https://doi.org/10.2514/1.T5608
8. Brown, C. and Bridges, J., "Small Hot Jet Acoustic Rig Validation," NASA-TM 2006-214234, April 2006.
9. Bridges, J. and Brown, C. A., "Validation of the Small Hot Jet Acoustic Rig for Aeroacoustic Research," AIAA Paper 2005-2846, May 2005.
10. Bridges, J. and Wernet, M. P., "Establishing Consensus Turbulence Statistics for Hot Subsonic Jets," AIAA Paper 2010-3751, June 2010.
11. Bridges, J. and Wernet, M. P., "The NASA Subsonic Jet Particle Image Velocimetry (PIV) Dataset," NASA-TM 2011-216807, Nov. 2011.
12. Rumsey, C., Smith, B., and Huang, G., "Description of a Website Resource for Turbulence Modeling Verification and Validation," AIAA Paper 2010-4742, June 2010.
13. Locke, R. J., Wernet, M. P., and Anderson, R. C., "Rotational Raman-Based Temperature Measurements in a High-Velocity Turbulent Jet," ***Measurement Science and Technology***, Vol. 29, No. 1, Dec. 2017.
14. DeBonis, J. R., "Prediction of Turbulent Temperature Fluctuations in Hot Jets," AIAA Journal, Vol. 56, No. 8, 2018, pp. 3097–3111, https://doi.org/10.2514/1.J056596.

15. Mielke, A., Elam, K., and Sung, C.-J., "Multi-property Measurements at High Sampling Rates Using Rayleigh Scattering," ***AIAA Journal***, Vol. 47, No. 4, 2009, pp. 850–862, https://doi.org/10.2514/1.37369 .
16. Wernet, M. P., Georgiadis, N. J., and Locke, R. J., "PIV and Rotational Raman-Based Temperature Measurements for CFD Validation in a Single Injector Cooling Flow," AIAA Paper 2018-3857, June 2018, https://doi.org/10.2514/6.2018-3857.
17. Spiegel, S., Borghi, M. R., and Yoder, D. A., "Large Eddy Simulations of a Single-Injector Cooling Flow Using the High-Order Flux Reconstruction Method," AIAA Paper 2022–1813, Jan. 2022, https://doi.org/10.2514/6.2022-1813 .
18. Borghi, M. R., "Implicit Large-Eddy Simulation of Single-Injector Cooling Flow," AIAA Paper 2022–1814, Jan. 2022, https://doi.org/10.2514/6.2022-1814 .
19. Yoder, D. A., "Assessment of Turbulence Models for a Single-Injector Cooling Flow," AIAA Paper 2022–1812, Jan. 2022, https://doi.org/10.2514/6.2022-1812 .
20. Borghi, M. R., Spiegel, S., Yoder, D. A., Georgiadis, N. J., and Wernet, M. P., "Turbulent Simulations of Cooling Jets in Crossflow," AIAA Paper 2022–1815, Jan. 2022, https://doi.org/10.2514/6.2022-1815 .
21. Wernet, M. P., Georgiadis, N. J., Locke, R. J., Thurman, D., Poinsatte, P., "PIV and Rotational Raman-Based Temperature Measurements for CFD Validation of a Perforated Plate Cooling Flow: Part I," NASA TM-2019-220227, https://ntrs.nasa.gov/api/citations/20190029113/downloads/20190029113.pdf, and AIAA Paper 2020-1230, Jan. 2020, https://doi.org/10.2514/6.2020-1230 .
22. Pesich, J.M., Georgiadis, N. J., Wernet, M. P., Locke, R. J., Thurman, D. R., Poinsatte, P. E., "PIV and Rotational Raman-Based Temperature Measurements for CFD Validation of a Perforated Plate Cooling Flow: Part II," AIAA Paper 2022-0084, Jan. 2022, https://doi.org/10.2514/6.2022-0084.
23. Pesich, J. M., Georgiadis, N. J., and Wernet, M. P., "Multiphysics Computational Analysis of a Perforated Plate Cooling Flow," AIAA Paper 2021-1447, Jan. 2021, https://doi.org/10.2514/6.2021-1447.
24. Benton, S.I., and Lamberson, S.E., "Analysis of the PAW-5 Nozzle Test Case with HPCMP CREATE-AV Kestrel," AIAA Paper 2022-0083, Jan. 2022, https://doi.org/10.2514/6.2022-0083.
25. Emory, M., Shunn, L., Bose, S., and Ham, F., "Wall-modeled Large Eddy Simulation with Conjugate Heat Transfer Leveraging Clipped Voronoi-diagrams for the PAW-5 Nozzle Test Case," AIAA Paper 2022-0635, Jan. 2022, https://doi.org/10.2514/6.2022-0635.
26. Zore, K., Aliaga, C., Shah, S., Stokes, J., Zori, L., and Makarov, B., "Conjugate Heat Transfer Simulations of a Nozzle Flow over a Film-Cooled Plate, ***Journal of Thermophysics and Heat Transfer***, Vol. 37, No. 2, 2023, pp. 404-423, https://doi.org/10.2514/1.t6595
27. Winkler, C.M., "BCFD Analysis for the 5th AIAA Propulsion Aerodynamics Workshop: Film Cooled Nozzle Results, AIAA Paper 2022-0085, Jan. 2022, https://doi.org/10.2514/6.2022-0085.
28. Georgiadis, N. J., Wernet, M. P., Crowe, D. S., Woeber, C. D., Karman-Shoemake, K.C., Winkler, C.M., "Assessment of Multiphysics Computations of Flow Over A Film Cooled Plate," ***Journal of Thermophysics and Heat Transfer***, Articles in Advance, Mar. 2025, pp. 1-19, https://doi.org/10.2514/1.t7062.
29. Seiner, J. M., Ponton, M. K., Jansen, B. J., and Lagen, N. T., "The Effect of Temperature on Jet Noise Emission," AIAA Paper 92-02-046, 1992.
30. Wernet, M. P., Georgiadis, N. J., and Locke, R. J., "Velocity, Temperature, and Density Measurements in Supersonic Jets," NASA/TM-20205007269, October 2020, https://ntrs.nasa.gov/citations/20205007269, (the entire raw data set is also available here)
31. Georgiadis, N. J., Wernet, M. P., Locke, R. J., and Eck, D. G., "Mach Number and Heating Effects on Turbulent Supersonic Jets," AIAA Journal, Vol. 62, No. 1, Jan. 2024, pp. 31-51, https://doi.org/10.2514/1.j063186.
32. Wernet, M. P., Georgiadis, N. J., and Locke, R. J., "Raman Temperature and Density Measurements in Supersonic Jets," Experiments In Fluids, Vol. 62, No. 3, 2021, pp. 1-21, https://doi.org/10.1007/s00348-021-03162-2
33. Georgiadis, N. J., Wernet, M. P., Winkler, C. M., Benton, S. I., and Connolly, B. J., "Summary of the 6th Propulsion Aerodynamics Workshop Nozzle Test Case: Heated Supersonic Axisymmetric Jets," AIAA Paper 2024-0749, Jan 2024, https://doi.org/10.2514/6.2024-0749.
34. Zore, K., Aliaga, C., Selva, J., Zori, L., Makarov, B., "High-Fidelity SBES Simulations for Supersonic Nozzle Flows, AIAA Paper 2024-0753, Jan. 2024, https://doi.org/10.2514/6.2024-0753.
35. Kramer, C. and Crowe, D. S., "Turbulence Model Assessment for Heated Supersonic Jets," AIAA Paper 2024-0750, Jan. 2024, https://doi.org/10.2514/6.2024-0750.
36. Winkler, C. M., "BCFD Analysis for the 6th AIAA Propulsion Aerodynamics Workshop: Nozzle Results, AIAA 2024-0752, Jan. 2024, https://doi.org/10.2514/6.2024-0752.
37. Potturi, A.S., Batten, P., Bachchan, N., and Peroomian, O., "Modeling of Turbulent Supersonic Jet Plumes Using CFD++," AIAA Paper 2024-0751, Jan. 2024, https://doi.org/10.2514/6.2024-0751.
38. Georgiadis, N. J., Dippold, V.F., Baurle, R.A., Rumsey, C.L., "Heated Supersonic Jet Cases for the NASA Turbulence Modeling Resource," AIAA Paper 2025-2577, Jan. 2025, https://doi.org/10.2514/6.2025-2577.

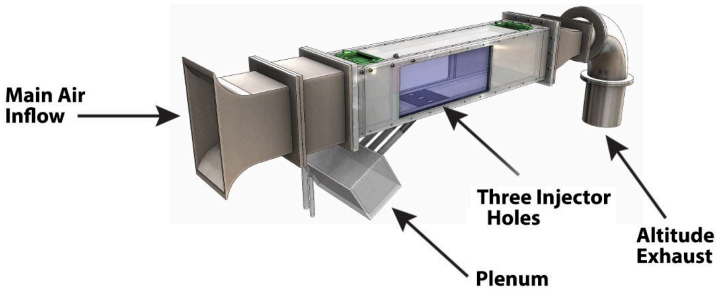


Figure 1.— GRC Film Cooling and Heat Transfer Facility (SW6)

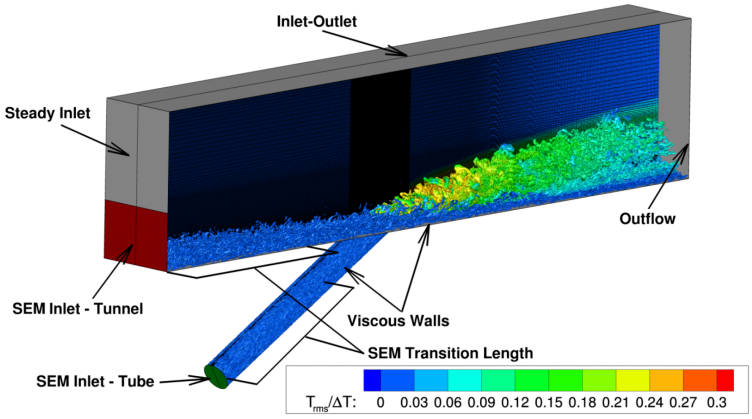
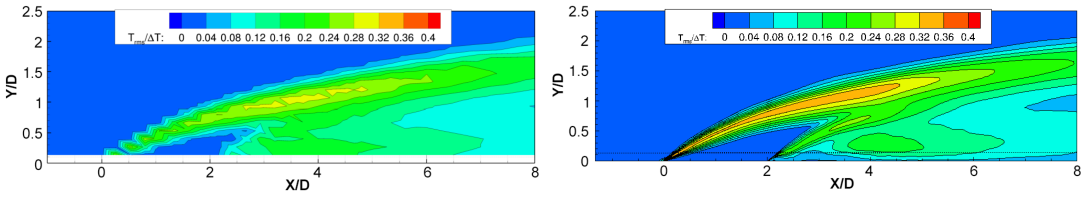


Figure 2.— Perspective view of LES computations for the THX Phase 1 cooling flow problem.



(a) Hot-wire measurements (b) LES

Figure 3.—Comparison of T-rms.

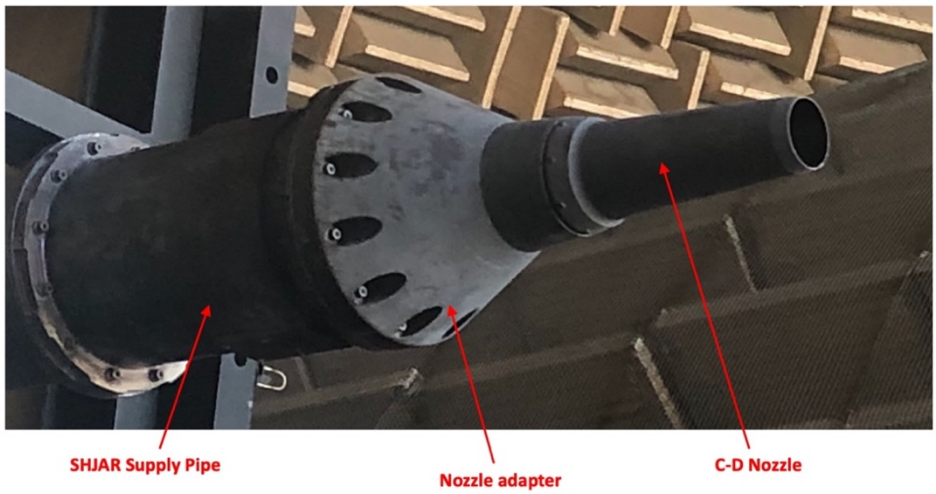
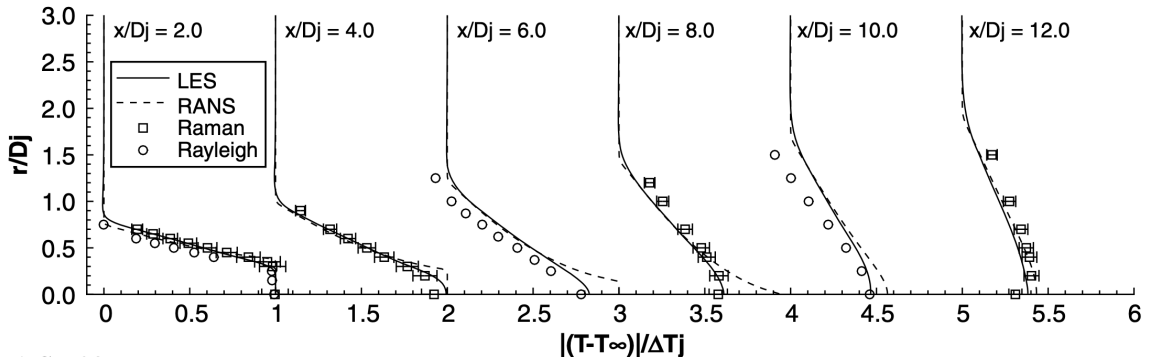
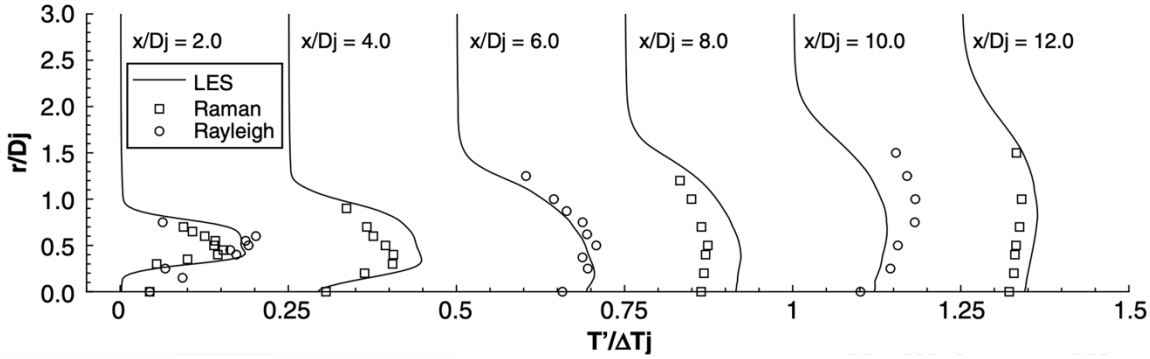


Figure 4.—Test rig (SHJAR) setup with C-D nozzle installed.



(a) Mean temperature



(b) rms of temperature

Figure 5.—Comparisons of temperature statistics for the THX – Phase 2 experiments.

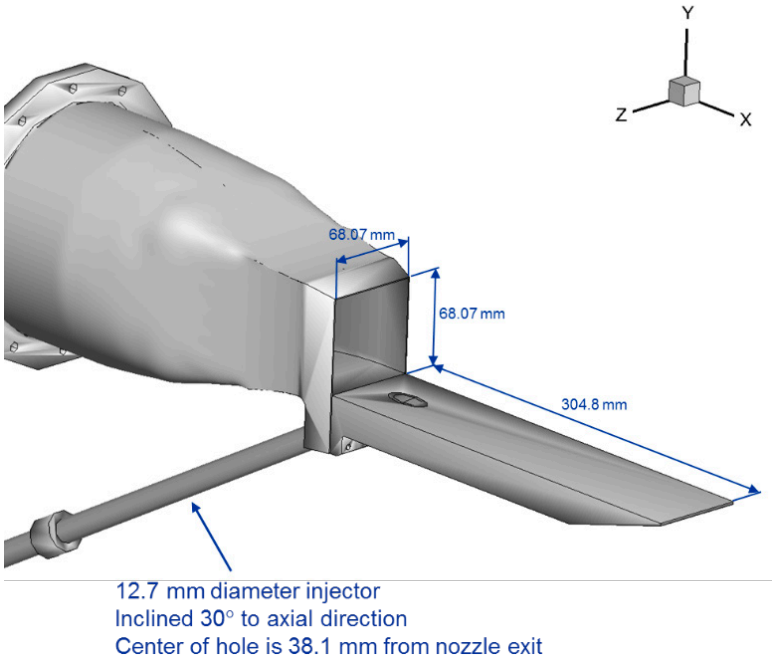
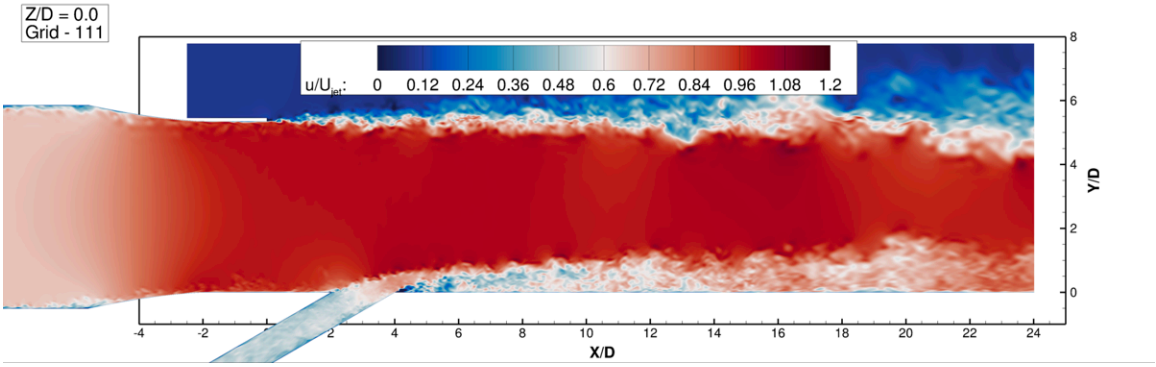
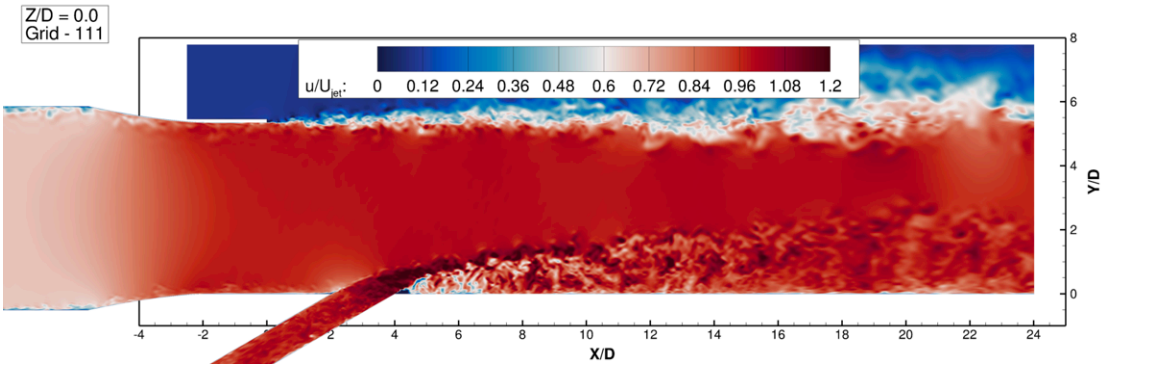


Figure 6.—THX – Phase 3 test configuration.



(a) BR = 1



(b) BR = 2

Figure 7.—Axial velocity contours from WRLES calculations using FDL3DI.

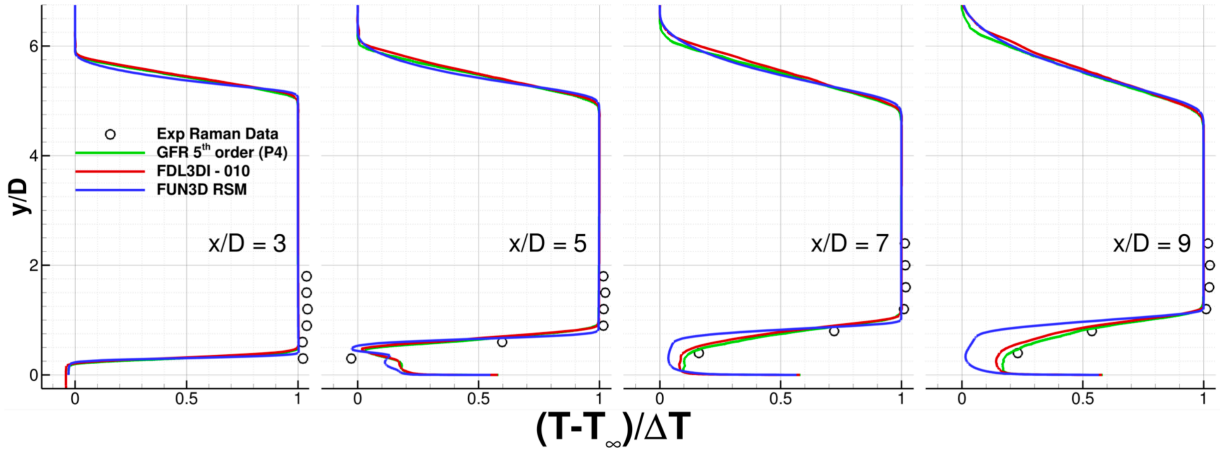


Figure 8.—Centerline mean temperature profiles; comparison of experiment to LES and RANS computations.

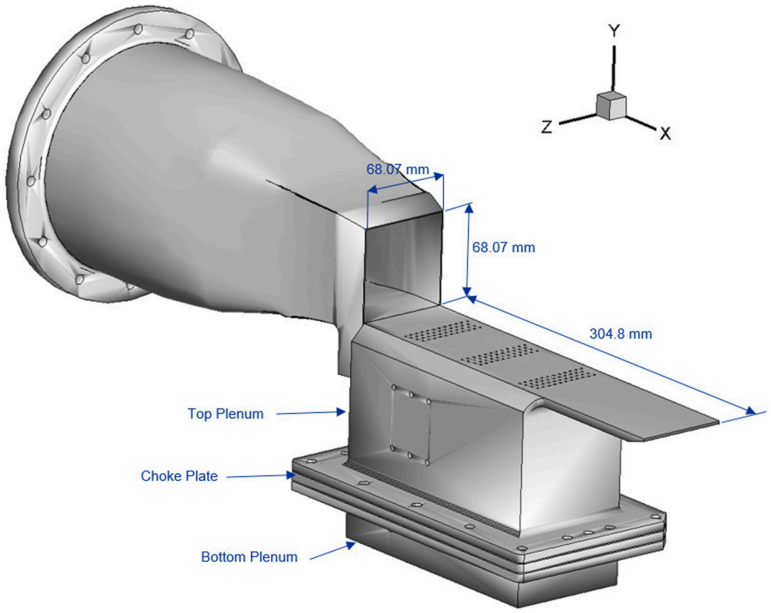


Figure 9.—THX – Phase 4 test configuration.

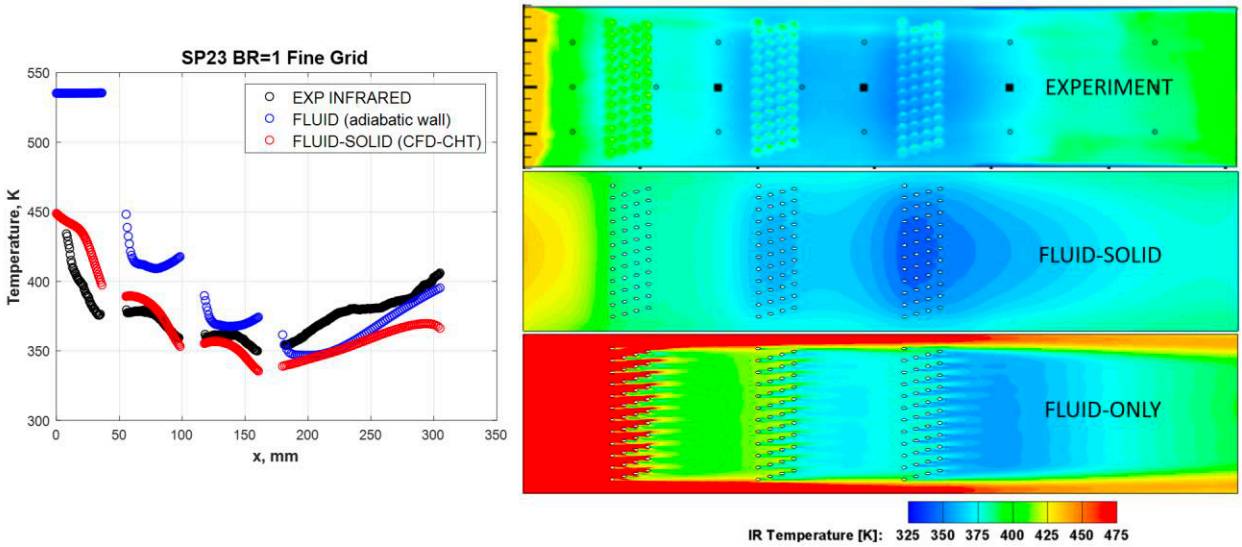


Figure 10.— Centerline temperature (left) and plate surface temperature contours (right) for BR=1.

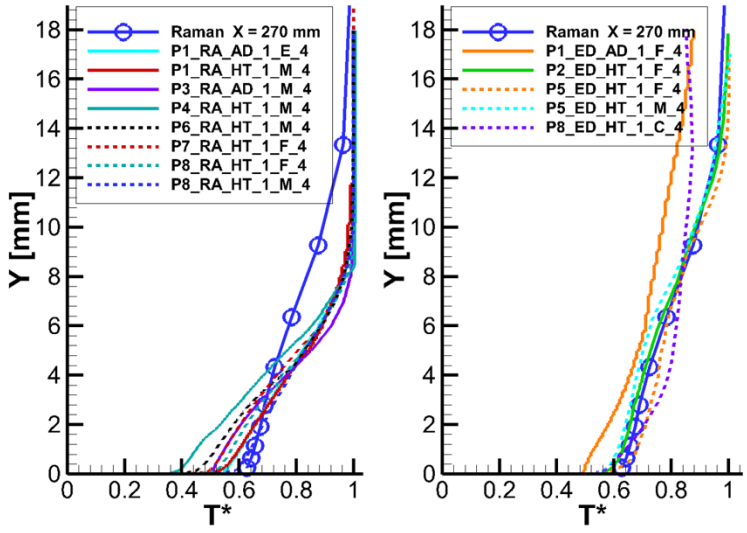


Figure 11.— Temperature profiles comparisons along the plate overhang (left-RANS, right-LES).

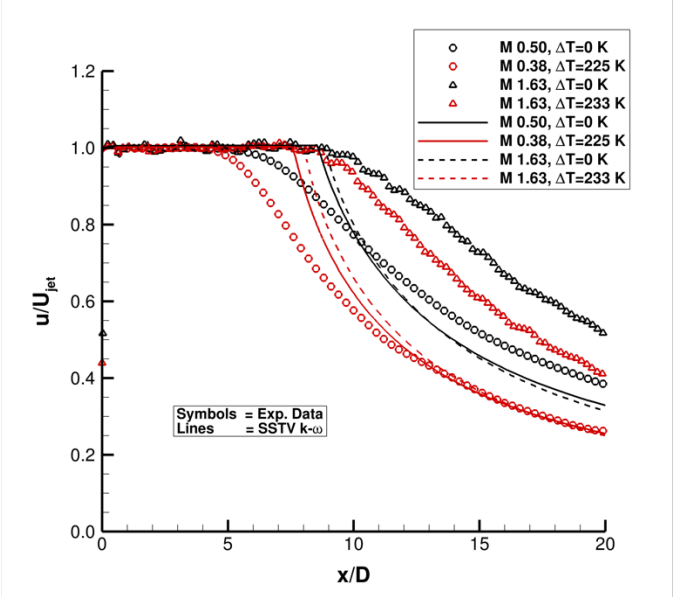
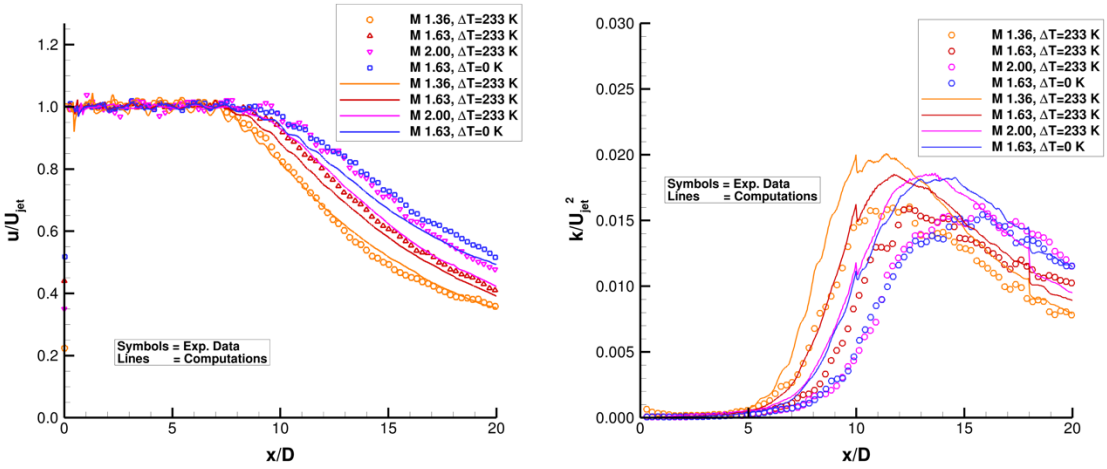
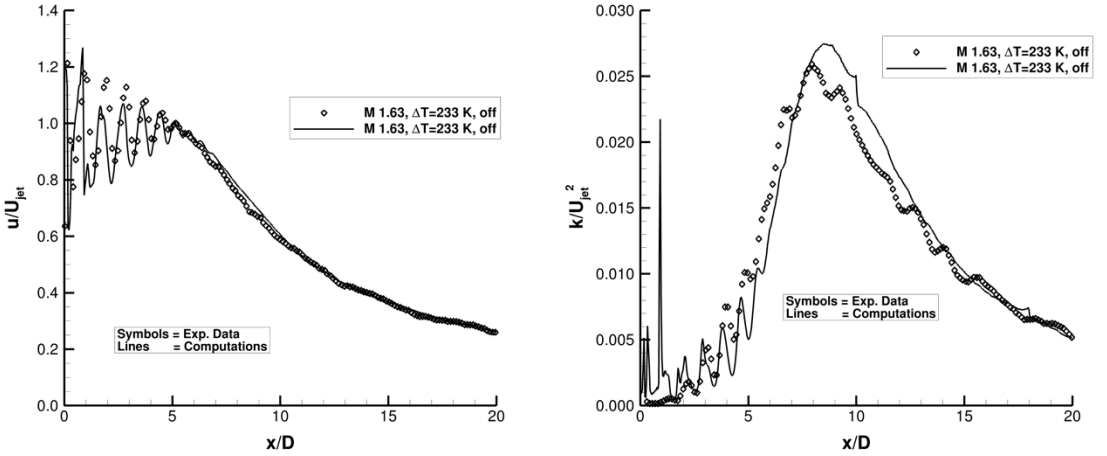


Figure 12.— Comparison of subsonic and supersonic round jets.



(a) axial velocity (b) turbulent kinetic energy

Figure 13.—Centerline velocity statistics for WMLES solutions, on-design cases.



(a) axial velocity (b) turbulent kinetic energy

Figure 14.—Centerline velocity statistics for WMLES solutions, off-design case.